Pressure induced metallization of fordite SnNb2O6 from first principles

Samir F. Matar, Mass A. Subramanian, Jean Etourneau

Accepted Dec. 2013/ In press/ *Computational Materials Science (Elsevier).*

Pressure induced Metallization of Fordite $SnNb_2O_6$ from First Principles.

S.F.Matar[a,b,*], M.A. Subramanian[c] , J. Etourneau[a,b]

[a]CNRS, ICMCB, UPR 9048, F-33600 Pessac, France
[b]Univ. Bordeaux, ICMCB, UPR 9048, F-33600 Pessac, France
[c]Oregon State University, Department of Chemistry, Corvallis, OR 97331-4003, USA.

Dedicated to Professor Gérard Demazeau on the occasion of his 70th birthday.

Abstract.

From DFT based calculations establishing energy-volume equations of state, a proposition of high pressure candidate structures with reduced volumes, namely columbite and trirutile are proposed for fordite mineral $SnNb_2O_6$. The key effect is the destabilization of divalent tin in fordite towards tetravalent state upon compression. This is helped with smaller size tetravalent tin. The remarkable electronic structure change is the transformation from semi-conducting fordite to metallic high pressure forms thanks to the electron transfer from Sn to Nb and O as quantified from charge density analyses.

Keywords:
Fordite mineral, DFT, high pressure, equation of states, density of states.

1. Introduction

The divalent state of Sn is not common in oxides. In spite of the existence of SnO, it is mostly tetravalent tin, Sn^{IV} which is encountered as in cassiterite mineral: SnO_2. Also divalent tin is less stabilized than in Pb compounds. In the context of the search for lead and bismuth free compounds for applications in actuators, respectful of the environment, we recently investigated the stability and ferroelectric properties of perovskite derived $SnTiO_3$ from first principles [1]. Indeed the large size of Sn^{II} could enable its location at the A corner sites in ABO_3 perovskite. However its synthesis has not been successful as yet.

Sn^{II} is found in the mineral fordite ($SnNb_{1.5}Ta_{0.5}O_6$) [2] and the synthesis of $SnNb_2O_6$ ternary oxide requires a reducing atmosphere to be obtained pure. It crystallizes in the monoclinic crystal system with *C*2/*c* space group SG and four formula units FU per unit cell. Sn is five-fold coordinated with oxygen with an average d(Sn-O) ~ 2.3 Å, which can be expected from the divalent state of tin: r(Sn^{II})= 1.12 Å, versus r(Sn^{IV}) = 0.70 Å. Actually the earliest structural studies erroneously proposed tin to be tetravalent in a modified stoichiometry $Sn^{IV}Ta_2O_7$ [3]. In fordite, niobium atoms are found in two non equivalent sites in a distorted octahedral coordination with oxygen. The average Nb-O length is ~2 Å. NbO_6 octahedra are edge sharing and form Nb_2O_{10} groups. These groups are corner sharing and run as Nb_4O_{12} files along *a* direction, i.e. parallel to (*b*, *c*) plane; they are separated by Sn (Fig. 1a).

In AB_2O_6 stoichiometry several divalent alkaline earth ANb_2O_6 such as A = Ca [4] crystallize in the columbite-type structure with orthorhombic space group (SG) *Pbcn* and four FU per unit cell. The structure shown in Fig. 1b is close to that of $SnNb_2O_6$ for the stacking of the octahedra. On the other side $FeTa_2O_6$ crystallizes in tetragonal trirutile ($P4_2/mnm$ SG) with two FU per unit cell [5]. In spite of the large number of compounds crystallizing in the columbite structure, the Sn member does not belong to them. Size considerations pertaining to the large ionic radius of Sn seem to play an important effect. This provides an exemplary case study of evaluating the pressure effects on the structure both from the crystallography point of view as well as from the electronic structure one. This pertains to search for potential high pressure (HP) phases on one hand and to investigate the changes in the electronic states of the *p* (Sn) and *d* (Nb) elements in such conditions on the other hand.

In this paper we investigate the columbite and trirutile structures as potential candidates for HP $SnNb_2O_6$, based on computations within the density functional theory DFT [6]. Note that cation defect perovskite model was considered based on $Ce_xNb_2O_6$ [7] in the preliminary

investigations but the geometry optimized volume was found much larger (504 $Å^3$/cell) than fordite $SnNb_2O_6$ (cf. Table 1). From geometry optimizations and energy quantities the energy-volume equations of states EOS are derived for the three structures leading to propose columbite and trirutile as HP forms. Analysis of the electronic structure shows drastic electronic effects pertaining to the oxidation of Sn and subsequent metallization.

2. **Computational details**

Within DFT, the Vienna ab initio simulation package (VASP) based on plane waves [8] allows geometry optimization and cohesive energy calculations. For this we use the projector augmented wave (PAW) method [8,9], with the generalized gradient approximation (GGA) scheme following Perdew, Burke and Ernzerhof (PBE) [10]. Preliminary calculations with local density approximation LDA [11] led to largely underestimated volumes versus the experiment. The conjugate-gradient algorithm [12] is used in this computational scheme to relax the atoms. The tetrahedron method with Blöchl corrections [9] as well as a Methfessel-Paxton [13] scheme are applied for both geometry relaxation and total energy calculations. Brillouin-zone (BZ) integrals are approximated using the special k-point sampling. The optimization of the structural parameters is performed until the forces on the atoms are less than 0.02 eV/Å and all stress components below 0.003 eV/$Å^3$. The calculations are converged at an energy cut-off of 500 eV for the plane-wave basis set with respect to the k-point integration up to $8 \times 8 \times 13$ (k_x, k_y, k_z) for best convergence and relaxation to zero strains. The calculations are scalar relativistic and assume spin degenerate total spins.

The all electrons scalar-relativistic augmented spherical wave (ASW) method [14, 15] is subsequently used for a full description of the electronic structure and the properties of chemical bonding based on the analysis of the overlap integrals S_{ij} with the crystal orbital overlap populations COOP following Hoffmann [16]. In the plots, positive, negative, and zero COOP indicate bonding, anti-bonding, and non-bonding interactions, respectively.

3. **Results and discussion**

3.1 Geometry optimizations and equations of state

The initial and optimized crystal structure results are given in Table 1. Starting atomic positions for Foordite $SnTa_2O_6$, are those of the initial paper [2] whereas for the candidate HP phases we started from $CoNb_2O_6$ [4] and $FeTa_2O_6$ [5] structural data. The calculated volume of fordite is slightly smaller than experimental value. Relatively good agreement with the

experimental data can be traced out for the atomic positions. In both columbite and trirutile structures the volumes show close magnitudes, systematically smaller than fordite volume. This trend lets suggest that the two hypothesized forms can be considered as candidates for high pressure transformation of fordite. Also it is interesting to note a decrease of the Sn-O shortest distance from 2.2 down to 1.9 Å. This should involve enhanced Sn-O bonding as argued upon in the next section. It will be shown that this is connected with a change in the electronic configurations.

The structural modifications can be better assessed from plotting the energy (E) volume (V), E = *f*(V) calculated around the optimized parameters in Table 1 for the three phases and establish the corresponding equations of states (EOS). The curves are gathered in Fig. 2. Besides the above finding of smaller volume columbite and trirutile $SnNb_2O_6$, confirmed here, the ambient pressure curve of foordite is found at lower energy than the other two curves (columbite and trirutile) which are very close together. The fits by Birch EOS [17] up to the third order:

$$E(V) = E_0(V_0) + \frac{9}{8}V_0B_0[(V_0/V)^{2/3} - 1]^2 + \frac{9}{16}B_0(B'-4)V_0[(V_0/V)^{2/3} - 1]^3$$

provide equilibrium parameters E_o, V_o, B_o and $B^{'}$ respectively for the energy, the volume, the bulk modulus and its pressure derivative. The obtained values with a goodness of fit $\chi^2 \sim 10^{-6}$ are displayed in the insert of Fig. 2. They confirm the trends inferred from the visual inspection showing that the columbite and trirutile structures are close, with the latter at lower energy (< 1 eV). Then the two forms can be considered as HP candidates for fordite. In all phases the pressure derivative of the bulk modulus B_0, B' is ~4, a value usually encountered in oxides [18].

The smaller volumes lead to ~30 GPa larger bulk moduli. The magnitudes can be used to provide an estimation of the pressure required for the transformation: P ~ 23 GPa. This can be achieved using a diamond anvil cell device [19].

3.2 Electronic configurations and electronic structures

We further assess these results by analyzing the charge density issued from the self consistent calculations using the AIM (atoms in molecules theory) approach [20] developed by Bader who devised an intuitive way of splitting molecules into atoms as based purely on the electronic charge density. Typically in chemical systems, the charge density reaches a minimum between atoms and this is a natural region to separate them from each other. Such

an analysis can be useful when trends between similar compounds are examined; they do not constitute a tool for evaluating absolute ionizations. The results of computed charges (*Q*) are such that they lead to neutrality when the respective multiplicities are accounted for; the obtained values for $SnNb_2O_6$ in the three forms are:

Fordite: *Q*(Sn)= +2.47; *Q*(Nb)= +3.31; *Q*(O1)= –1.72; *Q*(O2)= –1.41; *Q*(O3)= –1.42.

Columbite: *Q*(Sn)= +4.00; *Q*(Nb)= +2.99; *Q*(O1)= –1.71; *Q*(O2)= –1.82; *Q*(O3)= –1.46.

Trirutile: *Q*(Sn)= +4.00; *Q*(Nb)= +2.89; *Q*(O1)= –1.65; *Q*(O2)= –1.62.

Although the charge on Sn is 2+ in fordite, it is calculated close to divalent (Sn^{II}) and contrasts well with the large change of oxidation state of Sn to tetravalent (Sn^{IV}) in the two HP forms. The charge transfer is then towards niobium as well as oxygen. Schematically with pressure, Sn changes from divalent to tetravalent and the electrons (formally) transferred to Nb reduce it from pentavalent (Nb^{V}) to tetravalent (Nb^{IV}). This observation is only found in the Sn compound, i.e. in $FeTa_2O_6$ and in $CoNb_2O_6$ *per se*, the calculations confirm the divalent character of Fe/Co and the pentavalent character of Nb. The slightly larger reduction of Nb in trirutile candidate HP structure could be at the origin of its larger stabilization versus columbite.

The above observations should be of significant consequence on the changes of the electronic structures which are discussed from the electronic density of states DOS obtained with the ASW method using the optimized structure parameters (Table 1). The site projected DOS in the three forms are shown in Fig. 3. Low energy lying filled Sn *d* states are not shown. Visual inspection shows a difference between Fig. 3a exhibiting fordite as semi-conducting at room pressure with ~1.8 eV gap, contrary to the two proposed HP forms which are conducting thanks to the crossing of the lower part of Nb *d* states by the Fermi level E_F (Figs. 3b and 3c). Note that Nb being an early element of the 2^{nd} transition metal period, its little filled *d* states are centered above the top of the valence band (E_V) in Fig. 3a and E_F in Figs. 3b,c. Low energy lying Sn *s* states are found at the bottom part of the valence band with decreasing energies from -7 eV (Fig. 3a) to –9 eV (Fig. 3b) and -10 eV (FiG. 3c). The itinerant part of Nb states, oxygen and tin *p* states are found in ~5 eV broad band with the VB where the quantum mixing occurs leading to the chemical bonding. The ~1.8 eV band gap in Fig. 3a is found at lower energy in the other two subfigures. Then major changes are in a quasi rigid shift of the DOS to lower energies due to the larger filling of Nb *d* states upon reducing with extra

electrons transferred from Sn, leading to the metallization mainly caused by electrons from Nb *d* states.

Lastly we comment on the modification of the metal-oxygen bonding strengths upon going from the room pressure $SnNb_2O_6$ to the trirutile high pressure candidate. Preliminary plots for metal-metal bonding strength showed very small magnitudes as with respect to metal-oxygen. Fig. 4 shows for $SnNb_2O_6$ the comparative metal-oxygen chemical bonding regrouping all oxygen sites for the room pressure and the high pressure trirutile structures. The features of energy gap and metallization are observed as in the relevant DOS panels. As a common result the Nb-O COOP are larger than Sn-O due to the twice larger Nb equivalents in the unit cell. Whereas the Sn-O COOP are smeared over the valence band and present low intensity in room pressure fordite, large changes are observed in the trirutile exhibiting high magnitude Sn-O bonding COOPs in a narrow energy range from -8 to -7 eV. The metallization is concomitant with the onset of antibonding Nb-O COOP at E_F. In both panels the bonding COOP are followed at higher energy by small antibonding contribution with negative magnitudes within the valence band but the major antibonding COOP, mainly for Nb-O, are found within the conduction band. These qualitative results, especially for Sn-O enhanced bonding behavior reflect the observed changes in the interatomic distances with pressure.

4. **Concluding remarks**

From DFT based calculations establishing energy-volume equations of state, a proposition of high pressure candidate structures for fordite has been provided. The key effect is in the destabilization of divalent tin in fordite towards tetravalent state upon compression. This is helped with smaller size tetravalent tin. The remarkable electronic structure change is the transformation from semi-conducting fordite to metallic high pressure forms thanks to the electron transfer from Sn to Nb and O as quantified from charge density analyses. Insulating or semiconducting materials becoming metallic with applying external pressure are scarce and the major expected effect is usually connected with superconductivity as recently identified for alkali iron selenide compounds [21]. While experimental investigations are underway to validate our theoretical propositions and to test such effects, a question arises as to whether the compound remains stable under such pressure conditions and electrochemical changes.

Acknowledgements

Discussions with Prof. Gérard Demazeau are gratefully acknowledged. We thank the Conseil Régional d'Aquitaine and the MCIA-University of Bordeaux for computational facilities.

References.

[1] S.F. Matar, I. Baraille, M.A. Subramanian, Chem. Phys., 355 (2009) 43.

[2] T. Scott Ercit, P. Cerny, Canadian Miner. 26 (1988) 899.

[3] N.V. Maximova, V.V. Ilyukhin Sov. Phys. Cryst. 12 (1967)105.

[4] P. W. C. Sarvezuk, E. J. Kinast, C. V. Colin, M. A. Gusmao, J.B. M. da Cunha, O. Isnard.

J. Appl. Phys. 109, (2011) 07E160.

[5] S.M. Eicher, J.E. Freedan, K.J. Lushington, J. Solid State Chem. 62 (1986) 220.

[6] P. Hohenberg, W. Kohn, Phys. Rev. B 136 (1964) 864.

W. Kohn, L.J. Sham, Phys. Rev. A 140 (1965) 1133.

[7] C. Bridges, J. E. Greedan, J. Barbier, Acta. Cryst. B 56 (2000) 183.

[8] G. Kresse, J. Furthmüller, Phys. Rev. B 54 (1996) 11169.

G. Kresse, J. Joubert, Phys. Rev. B 59 (1999) 1758.

[9] P. E. Blöchl, Phys. Rev. B 50 (1994) 17953.

[10] J. Perdew, K. Burke, M. Ernzerhof, Phys. Rev. Lett. 77 (1996) 3865.

[11] D. M. Ceperley, B. J. Alder, Phys. Rev. Lett. 45 (1980) 566.

[12] W.H. Press, B.P. Flannery, S.A. Teukolsky, W.T. Vetterling, Numerical Recipes,

Cambridge University Press, New York (1986).

[13] M. Methfessel, A. T. Paxton, Phys. Rev. B 40 (1989) 3616.

[14] Williams AR, Kübler J, Gelatt CD. Phys Rev B 1979;19:6094.

[15] Eyert V. The Augmented Spherical Wave Method – A Comprehensive Treatment, Lecture Notes in Physics, Springer, Heidelberg, 2007.

[16] Hoffmann R. Angew Chem Int Ed Engl 1987;26:846.

[17] F. Birch, J. Geophys. Res. 83 (1978) 1257.

[18] S.F. Matar, G. Demazeau, M.H. Möller, R. Pöttgen. Chem. Phys. Lett., 508 (2011) 215.

[19] A. Jayaraman, Reviews of Modern Physics, 55 (1983) 65; and web ref.

http://serc.carleton.edu/NAGTWorkshops/mineralogy/mineral_physics/diamond_anvil.html

[20] R. Bader, Chem. Rev 91 (1991) 893.

[21] L. Sun et al. American Physical Society, APS March Meeting 2013, March 18-22, 2013, and P. Gao et al. arXiv:1209.1340 [cond-mat.supr-con]

Table 1 $SnNb_2O_6$: Experimental and (calculated) lattice parameters.

Foorderite C2/c #15
Sn (4*a*) 000 Nb, O1, O2, O3 (8*f*) *x,y,z* [2]
a = 17.093 (17.07) Å
b = 4.877 (4.92) Å
c = 5.558 (5.40) Å
β = 90.85° (90.67°)
V / 4 FU = 463.3 $Å^3$ (454 $Å^3$)

Atom	*x*	*y*	*z*
Sn	0	0.240 (0.24)	¼
Nb	0.330 (0.32)	0.258 (0.26)	0.328 (0.33)
O1	0.427 (0.43)	0.420 (0.43)	0.401 (0.41)
O2	0.357 (0.37)	0.042 (0.04)	0.069 (0.07)
O3	0.219 (0.22)	0.063 (0.06)	0.353 (0.35)

Columbite Pbcn #60
Sn (4*c*) 0y ¼ ; Nb, O1, O2, O3 (8*d*) *x,y,z*. Exp. data from $CoNb_2O_6$ [4]
a = 14.125 (14.55) Å
b = 5.701 (5.77) Å
c = 5.038 (5.20) Å
V / 4 FU = 405.69 $Å^3$ (436.56 $Å^3$)

Atom	*x*	*y*	*z*
Co (Sn)	0	0.158 (0.160)	¼
Nb	0.161 (0.167)	0.361 (0.355)	0.780 (0.769)
O1	0.094 (0.090)	0.372 (0.387)	0.447 (0.434)
O2	0.082 (0.079)	0.117 (0.122)	0.897 (0.912)
O3	0.238 (0.243)	0.151 (0.141)	0.594 (0.604)

Trirutile P4$_2$/mnm #136
Fe (Sn) (2*a*) 000; Ta (Nb) (4*e*) 00*z*, O1 (4*f*) *x,x*,0; O2 (8*j*) *x,x,z*. Exp. data from $FeTa_2O_6$ [5]

a = 4.794 (4.87) Å
c = 9.192 (9.17) Å
V = 211.25 $Å^3$ (217.65 $Å^3$)
V / 4 FU = 422.50 $Å^3$ (435.30 $Å^3$)

Atom	*x*	*y*	*z*
Fe (Sn)	0	0	0
Ta (Nb)	0	0	0.333 (0.347)
O1	0.307 (0.288)	0.307 (0.288)	0
O2	0.297 (0.293)	0.297 (0.293)	0.322 (0.328)

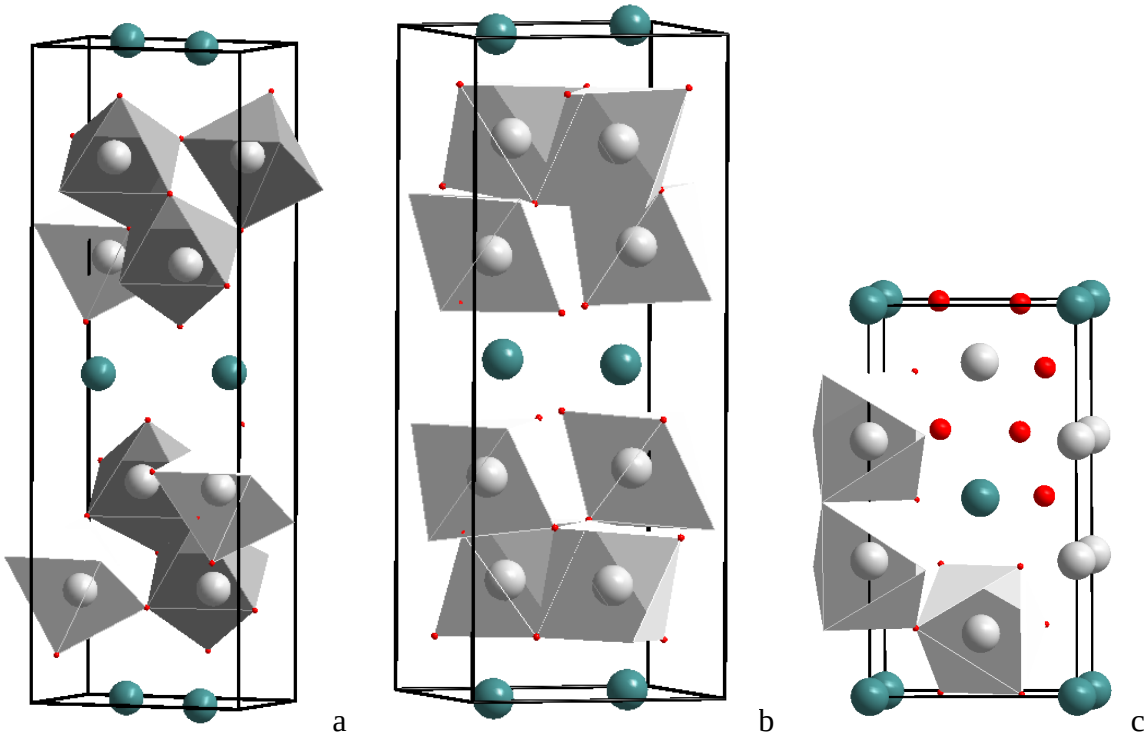

Fig. 1. $SnNb_2O_6$ structures. Room pressure Fordite a), and proposed high pressure Columbite b) and Trirutile c). Green, grey and red spheres represent Sn, Nb and O respectively.

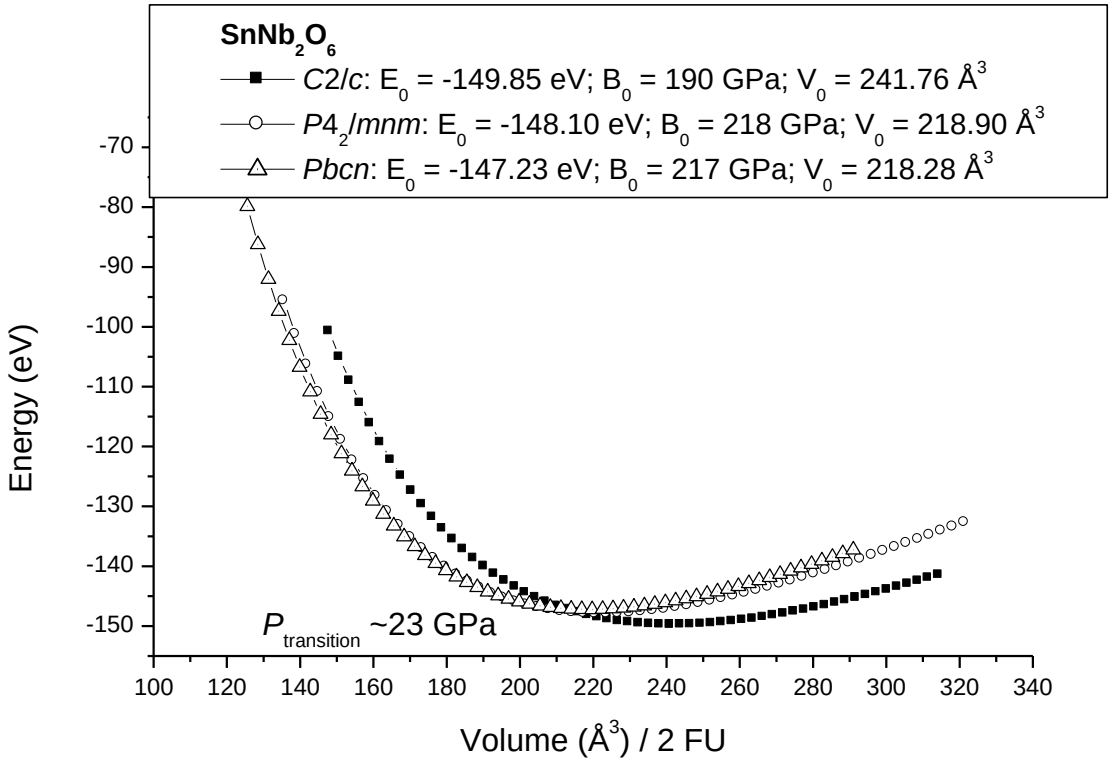

Fig. 2. $SnNb_2O_6$ E(V) curves for room pressure Foordite and high pressure Columbite and Trirutile. Fit values from Birch EOS are given in the insert.

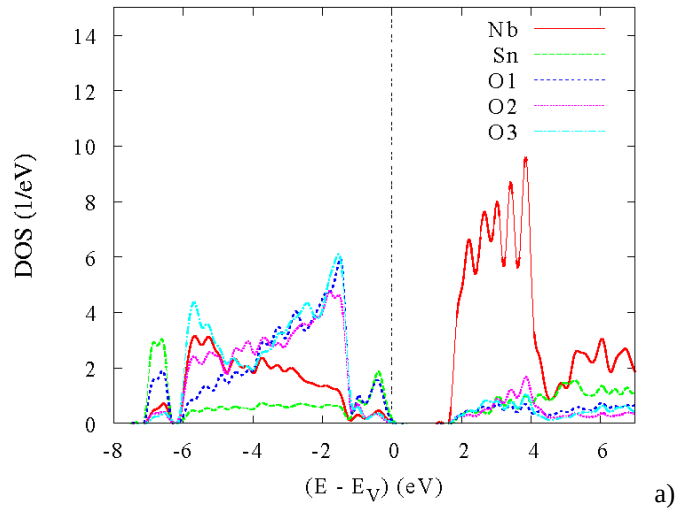

a)

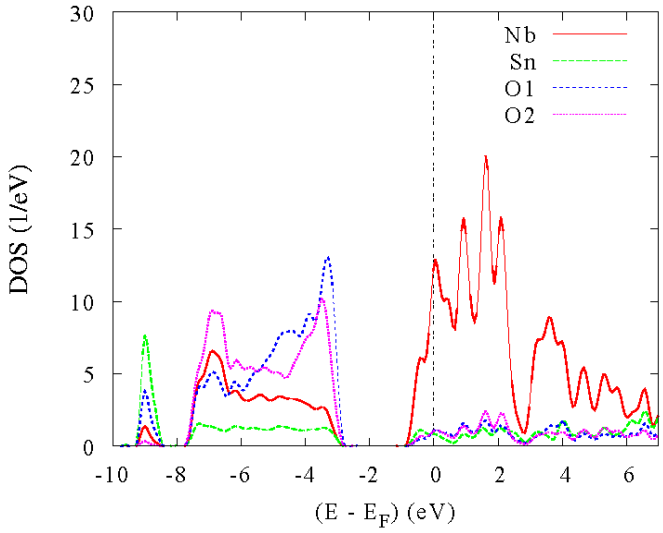

b)

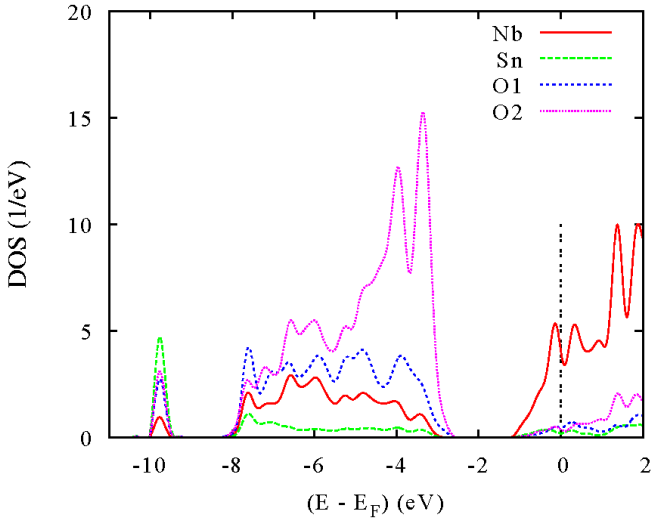

c)

Fig. 3: $SnNb_2O_6$ site projected DOS: a) Room pressure Fordite, b) HP Columbite, c) HP Trirutile.

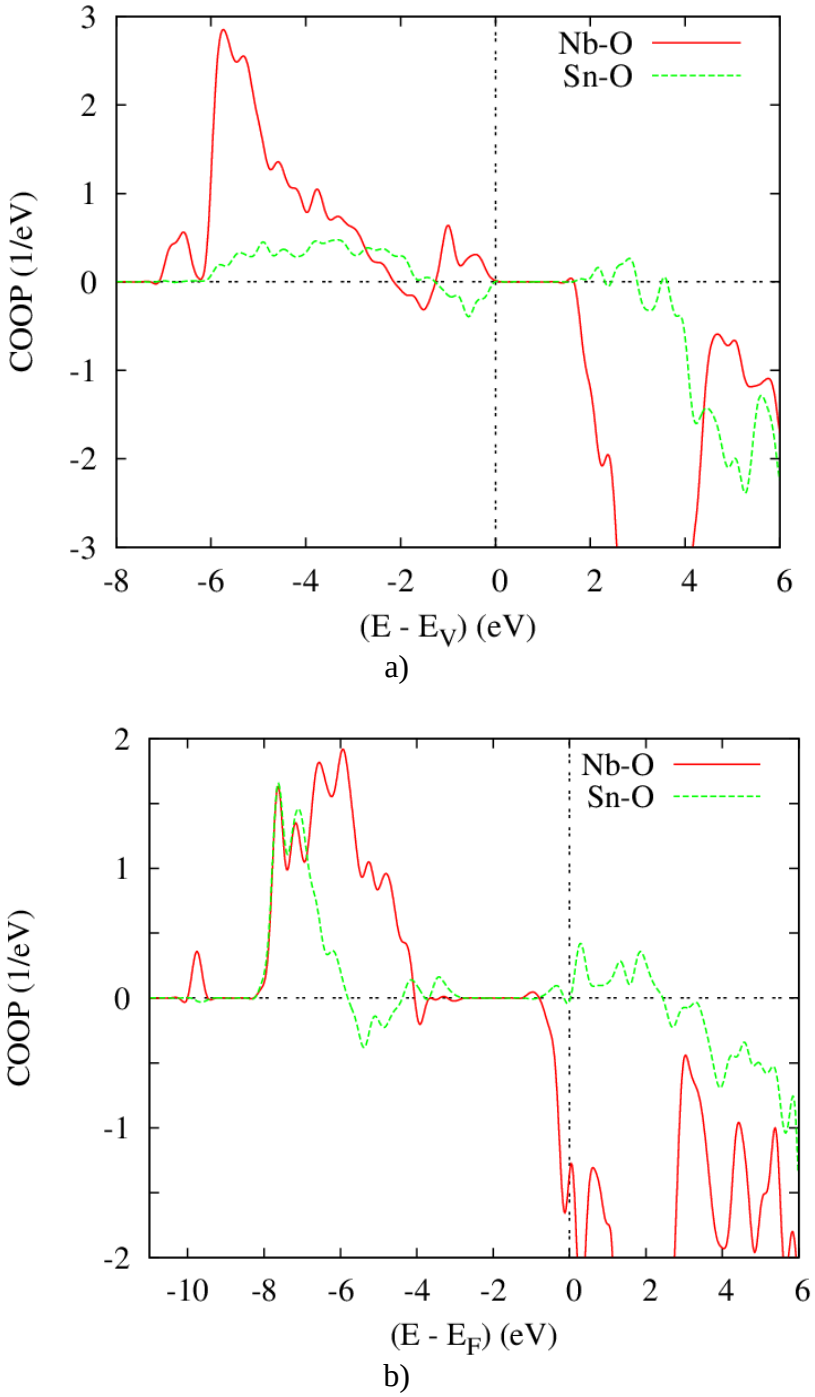

Fig. 4: Comparative metal-oxygen chemical bonding in a) room pressure $SnNb_2O_6$ and b) high pressure trirutile.